Journal of the European Ceramic Society 16 (1996) 825–831

0955-2219(95)00214-6
0955-2219/96/$15.00 + .00

Enhanced Toughness of a Partially Stabilised Zirconia at Elevated Temperatures

D. G. Jensen*

Department of Materials Engineering, Monash University, Clayton, Victoria, 3168 Australia

(Received 31 May 1995; revised version received 15 November 1995; accepted 29 November 1995)

Abstract

A ternary partially stabilised zirconia alloy has been developed by doping 10·8 mol% Mg–PSZ with 1·25 mol% CeO_2. This material has a microstructure that has oblate spheroidal precipitates that have twice the diameter and aspect ratio of those in Mg–PSZ. These precipitates, by enhancing toughening mechanisms other than the usual transformation toughening mechanism allow a considerable increment to toughening at elevated temperatures, despite transformation toughening not being operative at these temperatures. There is a measurable toughening at high temperature that cannot be attributed to transformation toughening. However, more work is required in the processing to reduce the porosity of the material.

1 Introduction

Optimally aged partially stabilised zirconia alloys at room temperature consist of a dispersion of metastable tetragonal precipitates in a cubic matrix. These precipitates transform to the monoclinic phase when some of the constraint imposed by the matrix is relieved by, for example, the nearby propagation of a crack. This transformation is accompanied by a 4% volume increase; the expansion of the precipitate absorbs some of the energy normally used in driving the crack and thus shields the crack tip from the crack driving force. Toughening of the material by this mechanism is known as transformation toughening.[1]

A significant limiting factor with this toughening mechanism is that an increase in the temperature of the material serves to stabilise the tetragonal phase, thus reducing the propensity for the precipitates to undergo a stress-induced transformation to the monoclinic phase.[2,3] This limits the service temperature of partially stabilised zirconias. In order to circumvent this problem, an attempt has been made to utilise other potential toughening mechanisms that are temperature insensitive to improve the high temperature toughness of PSZ-type materials, while retaining the transformation mechanism at low temperatures.

2 Background

With a view to retaining the transformation mechanism at room temperature, but tailoring the precipitate morphology in such a way as to enable other toughening mechanisms to become operative at high temperatures, we embarked on the development of an alloy that would incorporate precipitates having a morphology that would allow both of these aspects.

Toughening mechanisms other than transformation toughening that may benefit the toughness of PSZ-type materials at high temperature are crack deflection, particle pullout and crack bridging. Although particle pullout is a bridging mechanism, we will use the term to differentiate it from bridging where the bridge itself finally ruptures.

Crack deflection[4] serves to increase toughness by deflecting the crack out of its propagating plane, thereby increasing fracture surface area and, as the crack driving force and the crack direction no longer coincide, results in the decrease of the crack driving force. Faber & Evans[4] have proposed that increasing the aspect ratio of rod-shaped inclusions from 1 to 12 would serve to increment the toughness by 50%; their model is independent of particle size.

Crack bridging as used in our case[5,6] is a result of thermal expansion mismatch resulting in regions of residual compressive stress that result in these areas remaining intact following the passage of a crack, bridging the crack and serving to reduce the crack driving force until the bridge fails.

Particle pullout[7] utilises the frictional sliding energy loss that results from a particle being pulled out of the surrounding material in order to reduce the crack driving force; this continues until one side of

*Present Address: CSIRO Division of Wool Technology Geelong Laboratory, Belmont, Victoria, 3216, Australia.

the particle slides out of the surrounding material. It would obviously be desirable to have longer particles in order to maximise this contribution; however, it should be noted that very long particles would fail as opposed to frictionally sliding as the frictional force would be greater than the strength of the particle.

By carrying out calculations of potential toughening increments by the various mechanisms that would be operative at high temperature (crack bridging, particle pullout and crack deflection), it was determined that the ideal microstructure would be one in which the precipitates were large and had a high aspect ratio. To this end the calculation of precipitate morphologies by the minimisation of the elastic strain energy was carried out.

It is known that the metastable tetragonal precipitate's size is determined by solute content; in an attempt to maximise the solute in the precipitate, it was decided to use CeO_2 which has a high solubility in tetragonal zirconia. The precipitate, by having a higher solute content than Mg–PSZ, should remain tetragonal to a larger size than were there little solute present in the precipitate, as is the case for Mg–PSZ.

The aspect ratio of the precipitates is controlled by a combination of elastic anisotropy and the lattice parameter mismatch,[8] or 'tetragonality parameter':

$$t_1 = \frac{(a_t - a_c)}{(c_t - a_c)} \quad (1)$$

where a_c is the cubic lattice parameter, and a_t is the smaller and c_t is the larger of the tetragonal lattice parameters.

As zirconia has low elastic anisotropy,[9] it is the tetragonality parameter that dominates, and calculations show that a very low tetragonality parameter results in a high aspect ratio. For the system under investigation, the calculations based on the elastic constants at 1400°C given by Kandil *et al.*, and from lattice parameters derived from using Guinier XRD, an equilibrium aspect ratio of 7·7 is obtained; this is almost twice that obtained for Mg–PSZ.

3 Experimental

Powders in the ratio 1·25 mol% CeO_2, 10·8 mol% MgO and ZrO_2, to which was added 0·25 mol% SrO were attritter milled in a binder-isopropanol mixture for 6 h, thence spray-dried. This material is hereinafter referred to as 1·25 CM–PSZ. The resulting powder was then pressed into bars uniaxially at 30 MPa and the bars were then isostatically pressed at 200 MPa. These bars were then fired in an electric furnace at 1700°C for 2 h and cooled at 500°C/h to room temperature. Subsequent to this, the bars were aged for varying periods at 1400°C in order to allow precipitate growth and coarsening.

Mechanical testing was undertaken using an Instron 1122 with a crosshead speed of 0·1 μm/min for strength testing and 0·05 μm/min for toughness testing. A three-point rig with a span of 3 cm was employed for all testing, this rig was placed inside a furnace designed for high temperature testing when the high temperature (600°C) testing was carried out. Toughness testing was carried out in accordance with ASTM E399/83[10] for plane strain toughness testing; indentation toughness was carried out in accordance with the method of Anstis.[11]

For strength testing, bars were machined to about 40 × 4 × 2 mm; the tensile surface was polished to a mirror finish in order to remove the compressive zone as a result of grinding-induced surface transformation of the precipitates to monoclinic. The edges were chamfered to prevent cracks from propagating from the corners, which would give a false indication of the strength. Toughness testing was carried out using bars of the approximate dimension 40 × 8 × 4 mm, into which were cut notches 170 μm wide of various depths, in order to do single-edge, notched bend (SENB) testing. In order to remove the compressive zone at the notch tip, the bars were annealed at 1000°C for 20 min.

Scanning electron microscopy (SEM) was carried out in a Hitachi SF450 by observing the carbon coated fracture surfaces. Cracks propagating from the corners of Vickers indents on the polished surfaces of the sample aged 16 h were etched in HF for 4 min; the sample was then carbon coated for observation in the SEM. Transmission electron microscopy (TEM) was carried out using a Philips EM420 microscope, thin foils prepared by cutting a 5 mm diameter sample, thence thinning to 80 μm and then dimple grinding to 25 μm. Samples were then ion beam milled to perforation and given a light carbon coat. Precipitates were observed near the $<001>_c$ direction, the precipitate habit plane. Energy dispersive spectra (EDS) analysis was carried out in order to determine approximate solute content within the precipitates; no correction for absorption was carried out. The transformable tetragonal phase fraction was determined by the ratio of the areas under the {111} cubic/tetragonal and monoclinic X-ray peaks.[12]

4 Results and Discussion

4.1 Microstructural investigation

Observation of precipitates, and the measurement of precipitate diameter and aspect ratio has been documented elsewhere,[13] but the results are given in Table 1; additionally, we have added the solute content of the precipitates and the transformable tetragonal phase percentage.

Table 1. Comparison of various microstructural details of materials with regard to ageing time

Ageing time (h)	*MgO in precipitate. (MgO in 10·8 mol% Mg–PSZ)*	*Precipitate diameter (μm)*	*Precipitate aspect ratio*	*Transformable tetragonal (%)*
1	11·3 ± 0·7 (10·1) ± 1·0	0·167	4·39	2·3
4	11·8 ± 1.1 (5·9) ± 0·7	0·274	6.10	4·3
8	7·4 ± 0·5 (3·0) ± 0·6	0·371	6·30	5·2
16	3·8 ± 0·9 (0·8) ± 0·4	0·482	8·18	8·9

It should be noted that the CeO_2 concentration is remarkably stable at 1·3% in both the matrix and the precipitates for all ageing times. Additionally, the CeO_2 serves to reduce the diffusion of the MgO from the precipitates, which allows the precipitates to grow to a larger size before they have insufficient solute to remain tetragonal.

Comparing data for 9·4 mol% Mg–PSZ with those presented in Table 1, the diameter of precipitates in Mg–PSZ is about 0·2 μm and the aspect ratio is approximately 5 : 1; this illustrates the improvement in these morphological factors, which should result in improved high temperature toughness.[14,15]

4.2 Mechanical properties

The strength, although low in comparison to that for Mg–PSZ, shows an incremental increase with increasing ageing time to 4 h at room temperature, whereafter the strength reduces (see Fig. 1). Although the strength would be expected to reach a maximum after 16 h ageing (with Mg–PSZ, peak strength and toughness both coincide with peak ageing), the strengths of the samples aged for 4 h and 16 h do fall within experimental error. The samples tested at 600°C show a small rise with increasing ageing time to 16 h, whereafter the strength degrades. This degradation in strength of the materials aged for 32 h is due to the large (approximately 30%) monoclinic phase content in this overaged material. A feature worthy of comment is that the strength of material aged for 16 h tested at 600°C is very close to that of as-fired material tested at room temperature.

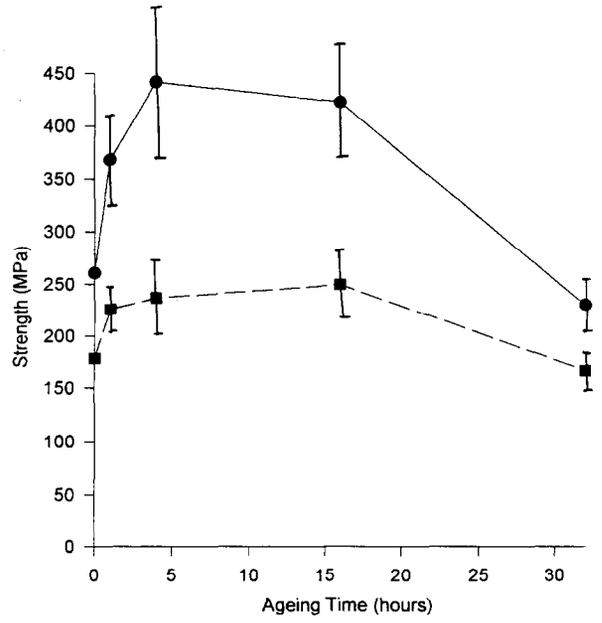

Fig. 1. Graph of strength versus ageing time. For all graphs, circles represent room temperature values, whereas squares represent measurements conducted at 600°C.

Toughness testing of these materials proved very interesting (see Fig. 2), firstly in that the toughness calculated by the indent method proved to be an underestimate of the true toughness measured. The materials show a considerable increment to toughness with increasing ageing time, both at room temperature and at 600°C. It should be noted that tests conducted at 800°C of samples aged for 4 h and 16 h gave the same toughness values as for 600°C (in other words, about 4·4 MPa$\sqrt{m}$). Swain *et al.*[2] have shown that for conventional Mg–PSZ, there is only about a 5% increment to toughening at 600°C, whereas our peak-aged material shows an increment of about 60%. Furthermore, the data given by Swain *et al.* show that the toughness for peak-aged Mg–PSZ at 600°C is less than that for as-fired material at room temperature. With regard to the decrease in toughness with increasing temperature, it is interesting that the toughness of eutectoid-aged Mg–PSZ decreases by about 50% when the testing temperature is increased to 600°C, whereas the decrease for 1·25 CM–PSZ is only about 33%. It should also be noted in Fig. 2(a) that the toughness of peak-aged 1·25 CM-PSZ at 600°C is measurably greater than that for as-fired material tested at room temperature. This would suggest that the proposed, non-transformation-based toughening mechanisms are at work. In order to validate this, it was decided to carry out an SEM evaluation.

4.3 SEM study

As fractography alone does not give an accurate indication of mechanisms, such as crack bridging

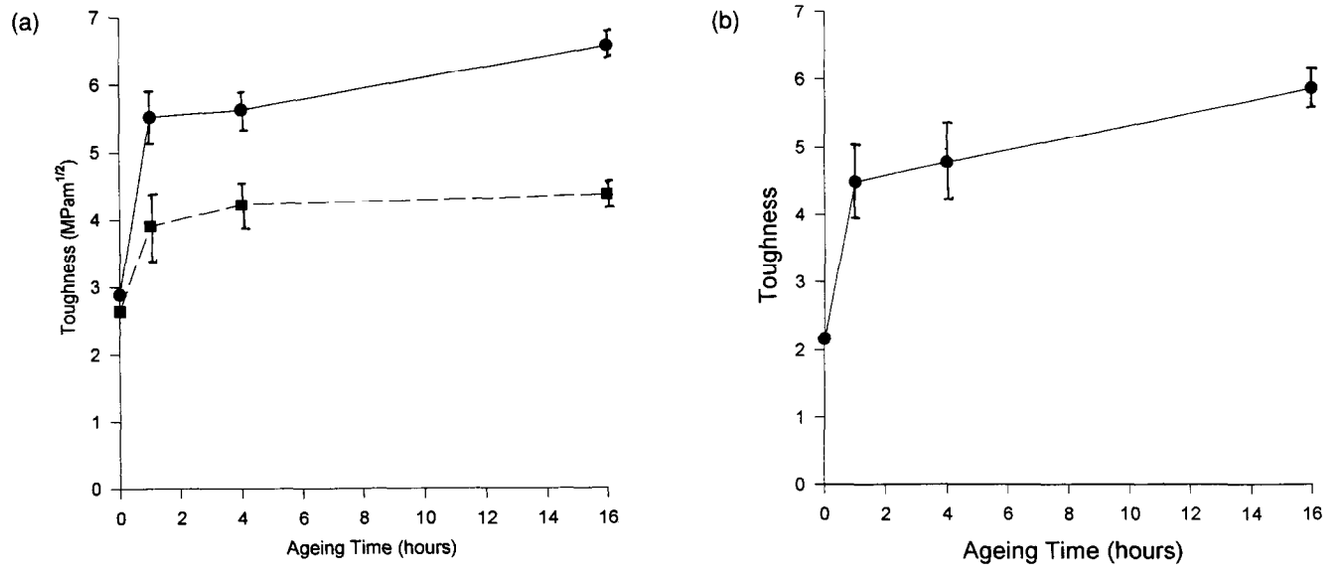

Fig. 2. (a) Graph of toughness versus ageing time, measured by SENB. The toughness of peak-aged CM–PSZ tested at 600°C is measurably greater than that of as-fired CM–PSZ tested at room temperature. (b) Graph of toughness versus ageing time for samples tested at room temperature by measuring the diagonal cracks emanating from a Vickers indent. Note that the toughness values obtained are an underestimate of the values obtained by using SENB.

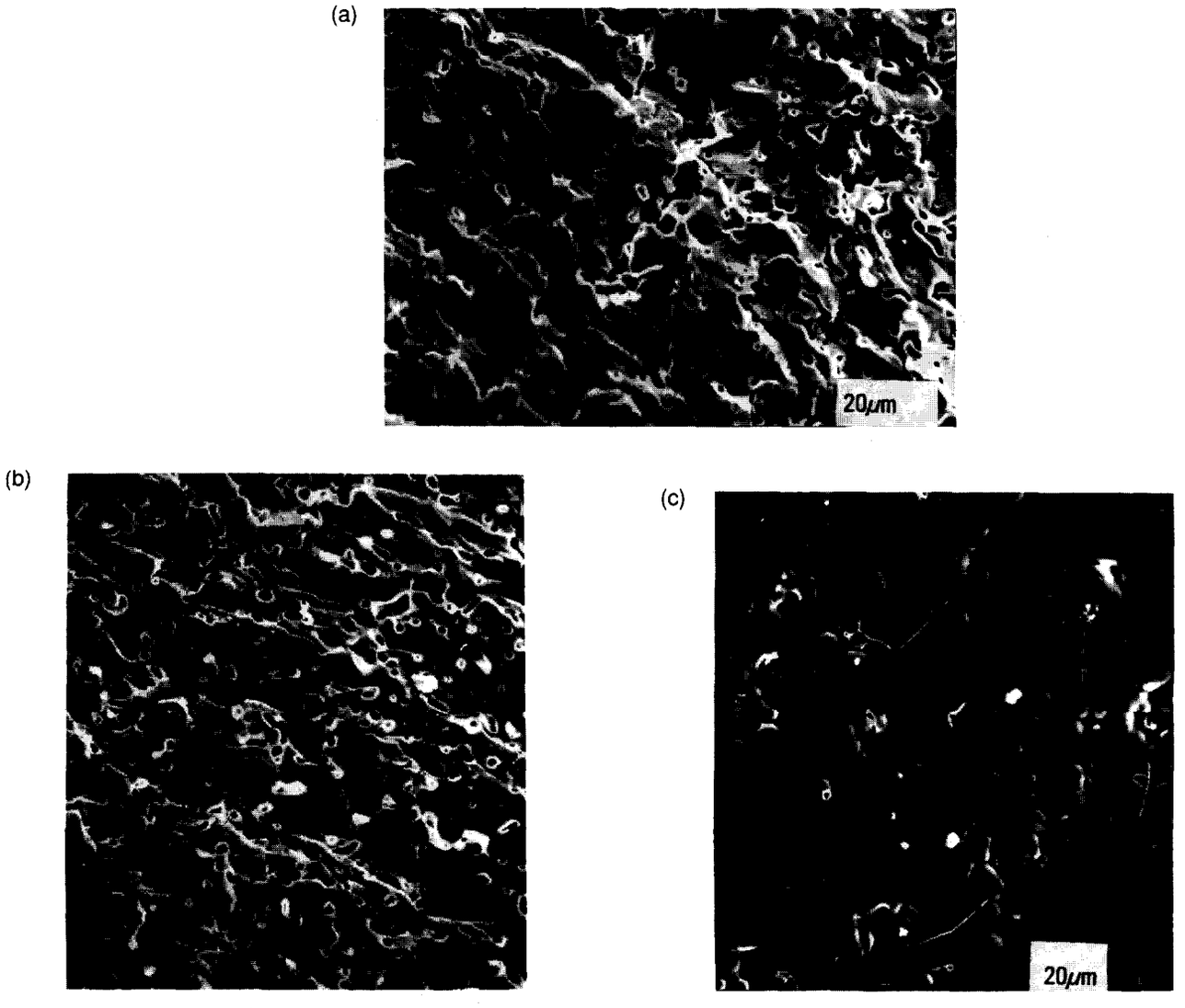

Fig. 3. (a) Fracture surface of as-fired material fractured at room temperature. Note the high apparent pore density exhibited by the preferred cleavage direction of the material. Both inter- and intra-granular fracture are evident. (b) Fracture surface of as-fired material fractured at 600°C. Notice the similarity of the fracture surface as compared with the material tested at room temperature. (c) Surface of diamond-sawn region of sample shown in (b). Note that the porosity is not as high as that for a fracture surface.

due to any bridges already having failed, it was decided also to study the cracks emanating from a Vickers indent in the aged 16 h sample in order to ascertain whether such processes were occurring.

Samples were found to have a grain size of 15–40 μm; the porosity was approximately 5% as measured by the comparison of measured and theoretical densities. The porosity was evenly distributed throughout the material.

It is interesting to note that the as-fired material exhibits cleavage-type fracture, with the preferred cleavage direction coinciding with that of the highest pore density. This is evident at both room and high temperatures (see Fig. 3), the true porosity of the bulk is not as high as is evident with the fracture surfaces (see Fig. 3(c)) resulting from the nature of the fracture.

Samples aged for 1, 4, and 16 h exhibit predominantly intra-granular fracture, and considerable crack–precipitate interaction is in evidence (see Figs 4, 5 & 6). This interaction clearly contributes to the enhanced toughness at high temperatures. Material aged for 32 h, having very large regions of grain boundary, monoclinic phase present, has predominantly intergranular fracture, which contributes to the reduced strength and toughness evident in this material (see Fig. 7).

The observation of cracks emanating from the corners of Vickers indents (see Fig. 8) provides evidence of crack deflection, precipitate pullout and crack

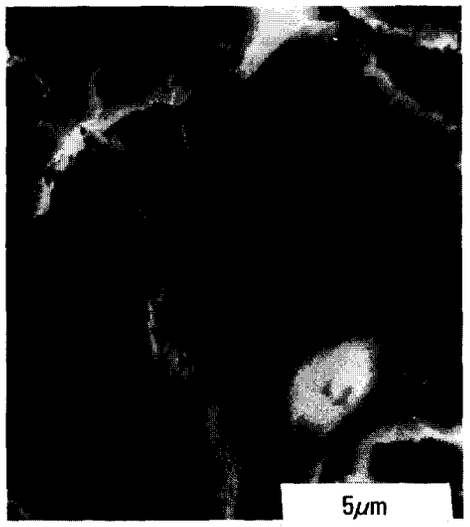

(a)

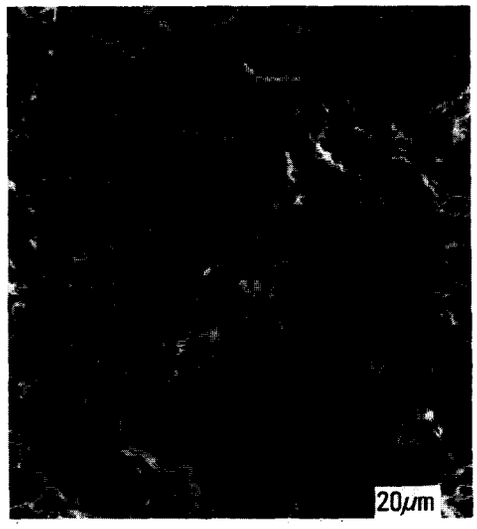

(b)

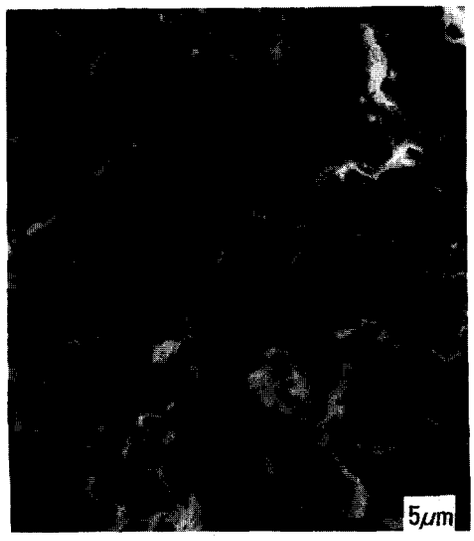

(c)

Fig. 4. (a) Fracture surface of material aged for 1 h fractured at room temperature. Note that there is considerable crack–precipitate interaction; the textured effect on the fracture surface is due to deflection of the crack about the precipitate. Some of the exposed precipitates could also be a result of crack bridging and pullout. Precipitates in the material aged for 1 h have approximately the same morphology as those in peak-aged Mg–PSZ. (b) Fracture surface of aged for 1 h material fractured at 600°C. Note that some of the fracture appears to have occurred inter-granularly, but that for intra-granular fracture, there is considerable crack–precipitate interaction. (c) Higher magnification micrograph of part of the region in (b), showing evidence of crack–precipitate interaction.

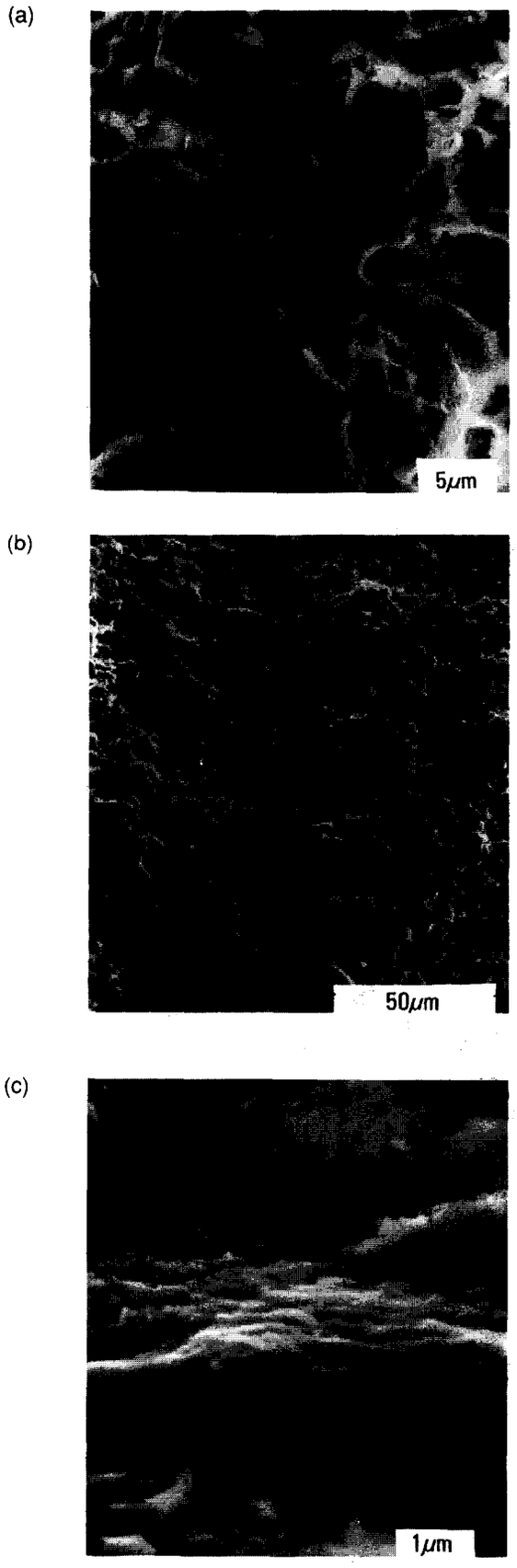

Fig. 5. (a) Fracture surface of material aged for 4 h fractured at room temperature. Most of the fracture is intra-granular, with some inter-granular fracture occurring. (b) Fracture surface of material aged 4 h fractured at 600°C. The fracture is primarily intra-granular. (c) Higher magnification micrograph of part of the region in (b). Note considerable crack–precipitate interaction; it is this type of interaction that accounts for the improved high temperature fracture toughness of this material.

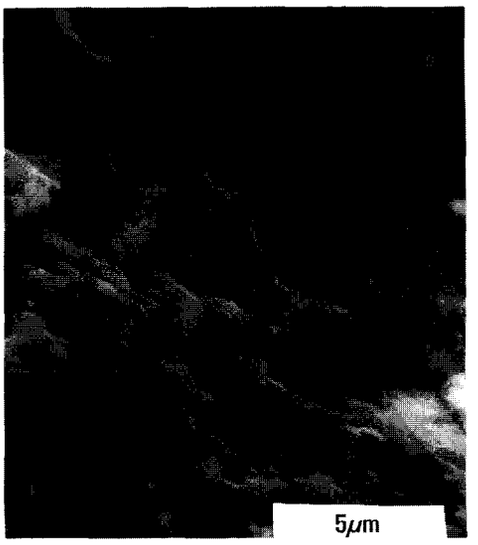

Fig. 6. Fracture surface of material aged for 16 h fractured at 600°C. Note the considerable extent of crack–precipitate interaction. Clearly, crack deflection has occurred, but it is difficult to say whether precipitate pullout has occurred, and impossible to tell whether crack bridging has occurred.

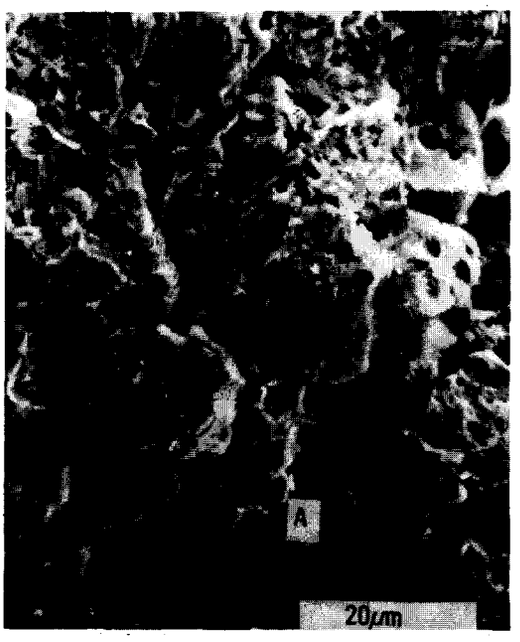

Fig. 7. Fracture surface of material aged for 32 h fractured at room temperature. Note that although there is some crack–precipitate interaction present, the fracture is predominantly inter-granular, and that there are regions of grain boundary monoclinic phase (A) through which the crack has preferentially propagated.

bridging. With regard to crack bridging, both elastic and plastic bridging elements are in evidence. These mechanisms, as previously discussed, are all temperature insensitive toughening mechanisms, and as such could be expected to contribute to the enhanced high temperature toughness evident in this material.

Another feature that is worthy of comment is that of the apparent morphology of many of the precipitates in Fig. 8. Although it appears that many of the precipitates have a kinked morphology, TEM observations point to these precipitates being the

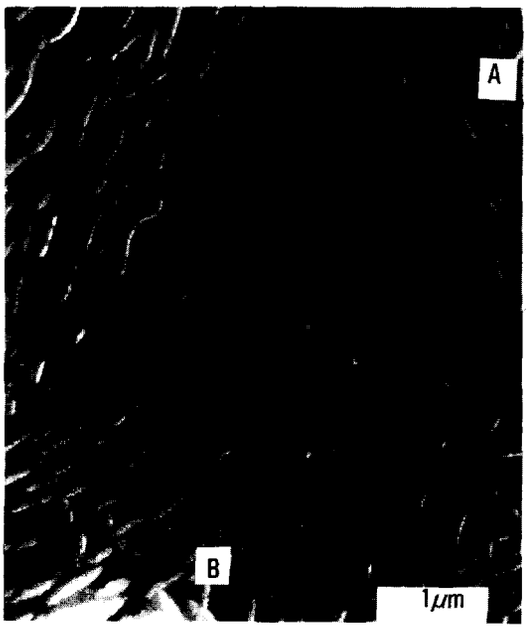

(a)

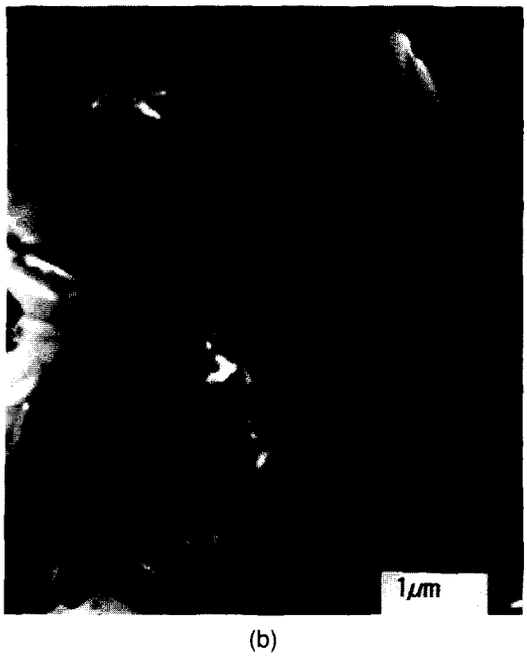

(b)

Fig. 8. Crack emanating from the corner of a Vickers indent in material aged for 16 h. (a) Particle pullout (A) and crack deflection (B) are clearly in evidence. (b) Crack bridging.

result of precipitates that have nucleated and grown in a rafted manner, having grown together.[13,14] In detail, however, the precipitates have been shown to deviate from an assumed oblate spheroid shape, but not to the extent as it appears in the SEM images.

5 Conclusions

(1) The high-temperature toughness shows a considerable increase with increasing ageing time giving promise to PSZ-type ceramics that may be used for high-temperature applications. The toughening increment at room temperature is similar to that for eutectoid-aged Mg–PSZ.

(2) Improved processing is required to reduce the porosity in order to improve the strength of the material.

(3) Sub-eutectoid ageing should improve the increment to transformation toughening in the same way as for Mg–PSZ.

Acknowledgements

The author wishes to acknowledge Alan White, who cut the notches in the toughness testing samples. The helpful advice of Professor Paul Rossiter and Associate Professor Trevor Finlayson is gratefully acknowledged, as is the critical reading of the document by Trevor. Much of this work was carried out at the CSIRO Division of Materials Science and Technology. This work was supported by an APA Award.

References

1. Green, D. J., Hannink, R. H. J. & Swain, M. V., *Transformation Toughening of Ceramics*, CRC Press, Boca Raton, FL, 1989.
2. Swain, M. V., Hughan, R. R., Hannink, R. H. J. & Garvie, R. C., *Magnesia-Partially-Stabilised Zirconia (Mg–PSZ) Microstructure and Properties*. Zirconia Conference, Japanese Ceramic Soc., Tokyo Inst. Tech., 1983.
3. Becher, P. F., Swain, M. V. & Ferber, M. K., Relation of Transformation Temperature to the Fracture Toughness of Transformation-Toughened Ceramics. *J. Mat. Sci.*, **22** (1987) 76.
4. Faber, K. T. & Evans, A. G., Crack Deflection Processes, *Acta Metall. Mater.*, **31** (1983) 565.
5. Knehans, R. & Steinbrech, R. W., Memory effect of crack resistance during slow crack growth in notched Al_2O_3 bend specimens. *J. Mat. Sci. Lett.*, **1** (1982) 327.
6. Rodel, J., Interaction Between Crack Deflection and Crack Bridging. *J. Eur. Cer. Soc.*, **10** (1992) 143.
7. Lange, F. F., *Fracture Mechanics and Microstructural Design, Fracture Mechanics of Ceramics*, Vol. 4, Plenum Press, New York, 1978, p. 799.
8. Khachaturyan, A. G., *Theory of Structural Transformations in Solids*, Wiley, NY, 1983.
9. Kandil, H. M., Greiner, J. D. & Smith, J. F., Single Crystal Elastic Constants of Yttria-Stabilized Zirconia in the range 20 to 700°C. *J. Am. Cer. Soc.*, **67** (1984) 341.
10. Srawley, J. E., Wide Range Stress Intensity Factor Expressions for ASTM E399 Standard Fracture Toughness Specimens. *Int. J. of Fracture*, **12** (1976) 474.
11. Anstis, G. R., Chantikul, P., Lawn, B. R. & Evans, A. G., A critical evaluation of indentation techniques for measuring fracture toughness. I. Direct crack measurements. *J. Am. Cer. Soc.*, **64** (1981) 533.
12. Garvie, R. C. & Nicholson, P. S., Structure and thermomechanical properties of Partially Stabilised Zirconias in the CaO–ZrO_2 system. *J. Am. Cer. Soc.*, **55** (1972) 152.
13. Jensen, D. G., Estimation of the Size Distribution of Spherical, Disc-like or Ellipsoidal Particles in Thin Films. *J. Phys. D.*, **28** (1995) 549.
14. Jensen, D. G., The orientation relationship between tetragonal zirconia precipitates with regard to elastic interaction energy, *J. Mat. Sci.*, **30** (1995) 5681.
15. Lanteri, V., Mitchell, T. E. & Heuer A. H., Morphology of Tetragonal Precipitates in Partially Stabilized ZrO_2. *J. Am. Cer. Soc.*, **69** (1986) 564.